

Air Flow Distribution through an A-Shaped Evaporator under Dry and Wet Coil Conditions

David A. YASHAR^{1*}, Piotr A. DOMANSKI²

¹The National Institute of Standards and Technology,
Gaithersburg, Maryland, USA
Tel: 301-975-5868, Fax: 301-975-8976, E-mail: dyashar@nist.gov

²The National Institute of Standards and Technology,
Gaithersburg, Maryland, USA
Tel: 301-975-5877, Fax: 301-975-8976, E-mail: pad@nist.gov

* Corresponding Author

ABSTRACT

This paper presents a study of the air flow distribution through a residential air-conditioning heat exchanger. The test subject was a finned-tube, A-shaped coil outfitted with a condensation collection pan required for horizontal installation. We examined the air flow distribution approaching and exiting the coil at the rated and a reduced air flow rate, and at two humidity levels. Our measurements showed that the presence of the condensation collection hardware greatly impedes air flow through the lower slab of the coil. Our measurements also uncovered portions of the coil where the airflow is blocked by the mounting hardware. The wet coil tests showed that the presence of water on the coil causes a large increase in air flow resistance which has an effect on the flow distribution. The distribution of water concentration was non-uniform and time dependent. We also developed a computational model of the flow through the test coil, based on a momentum resistance modeling approach.

1. INTRODUCTION

Finned-tube heat exchangers are the predominant type of heat exchangers used in comfort cooling applications. These heat exchangers are made up of a bundle of several dozen interconnected tubes, each of which is itself a single tube cross flow heat exchanger subject to a specific portion of the total air flow. The performance of the heat exchanger as a whole is the aggregate performance of each individual tube; therefore, it is strongly influenced by the air flow incident to every tube, or the air flow distribution to the heat exchanger.

Chwaloski et al. (1989) have shown that the air flow distribution in typical residential applications is far from uniform. Payne et al. (2003) demonstrated that the air-side nonuniformity can impose a large reduction in heat exchanger capacity, as much as 30 % in extreme cases. A series of studies by Domanski et al. (2004) and Domanski and Yashar (2007) involving the recent developments in machine learning have demonstrated that the capacity degradation due to air-side non uniformity can be, to a large degree, eliminated by designing the heat exchangers tube circuitry for the known air flow distribution. These studies highlight the fact that knowledge of the air flow distribution is essential to design a highly efficient heat exchanger because the air flow distribution influences the air-side heat transfer parameters at every location in the heat exchanger, and that the circuitry can be designed to optimally pair the refrigerant and air heat transfer potentials at each location.

Preliminary measurements on three finned-tube heat exchangers by Yashar et al. (2008) demonstrated that Particle Image Velocimetry (PIV) can uncover detailed air flow patterns that cannot be registered by traditional measurement methods. The goal of the present study is to use PIV to make high accuracy measurements and

validate Computational Fluid Dynamics (CFD) based models for predictions of air velocity profiles for a residential air-conditioning coil operating under real world conditions. The present study is based upon a two-slab finned-tube indoor heat exchanger. The study examines how the air flow distribution differs when operating at the rated and reduced air flow rate, and how the air flow distribution is affected by water present on the heat exchanger surface.

2. EXPERIMENTAL SETUP

The test coil used in these experiments is a 3-ton residential air-conditioning finned-tube heat exchanger. It consists of two slabs configured in an A-shape with an apex angle of 40 degrees. Each slab is made up of 60 tubes located in three depth rows with wavy fins, a detailed description of the test coil can be found in Yashar and Domanski (2009). The heat exchanger was outfitted with all of the required hardware to collect the water condensation from the coil, as shown in Figure 1, which consists of a plastic tray underneath the coil and a metal sheet positioned at an angle downstream of the coil to direct water droplets back to the drainage port. It is important to note the position and geometry of this hardware because it is located in proximity to the back side of the lower heat exchanger slab and therefore interferes with the air flow through the lower slab. The heat exchanger is also fastened to a mounting bracket, which is necessary to hold the angle between the two slabs and to fix the position of the heat exchanger within the duct. The design of this mounting bracket is such that it partially obstructs the air inlet side to both slabs of the heat exchanger, as indicated by the ellipse in Figure 1.

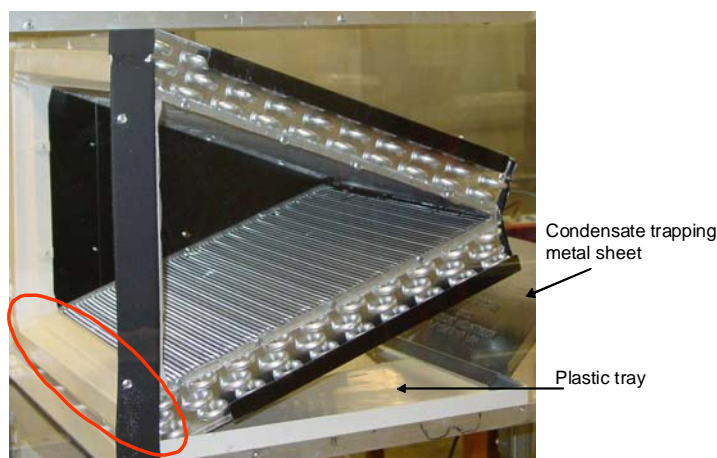


Figure 1 Test Coil

The heat exchanger was installed horizontally in a plexiglass duct. Cold water was pumped through the heat exchanger, with the same flow rate delivered to each slab. The water temperature difference was measured between the entrance and exit of each slab of the heat exchanger, which allowed us to calculate the heat transfer from each slab of the heat exchanger independently using the water enthalpy method. Conditioned air was drawn into the plexiglass test section using a blower downstream of the test section controlled by a variable speed motor. The air flow rate was measured according to ASHRAE Standard 37 (1998) using a nozzle located between the test section and the blower.

The PIV measurement system consisted of a theater style fog generator to produce particles that could be traced through the coil, a pair of Class IV pulsed lasers outfitted with a sheet forming optical lens to illuminate the fog particles, a double framed CCD camera to record the position of the particles, and a Programmable Timing Unit controlled by a personal computer to synchronize the operation of all of the components. A detailed description of all of the PIV equipment can be found in Yashar and Cho (2007).

The position of the PIV equipment relative to the test section varied for different measurements. Figure 2 illustrates the data collection method for measuring the air flow distribution approaching the inlet of the coil. In this configuration, the lasers are positioned in front of the test section and the laser light is projected as a sheet onto the inlet surface of the coil. The camera is located to the side of the test section, facing the illuminated plane that intersects the heat exchanger. In this manner, the position of fog particles at each laser pulse is recorded by the

camera, and the velocity field is calculated by mapping the motion of the fog particles between successive laser pulses.

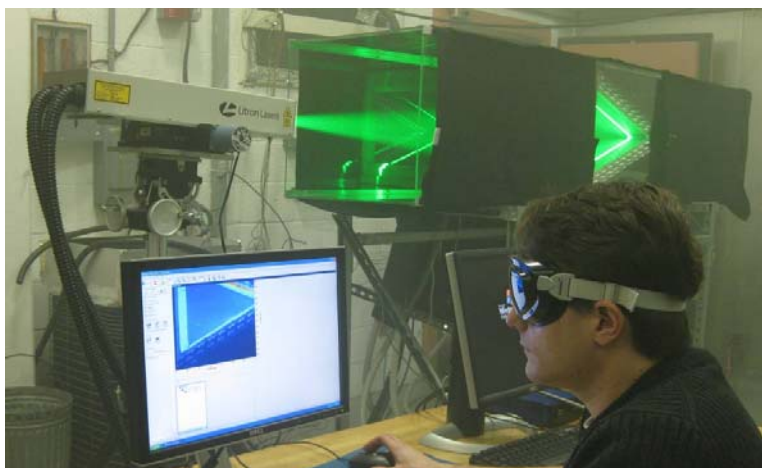


Figure 2 PIV Data Collection for Inlet Air Velocity Profile

The test matrix with varied parameters is shown in Table 1. The varied parameters were the inlet air dew point and flow rate to examine the effects of water vapor condensation and air flow rate on the air distribution. The constant target parameters for all tests were the inlet water temperature of 7.2 °C (45 °F) delivered to each slab at a rate of 285 g s⁻¹ and the inlet air dry-bulb temperature of 26.7 °C (80 °F).

Table 1 PIV Measurement Test Matrix

Test	HX Slab	HX Face	Air Flow Rate	Inlet Air Dew Point
1a	Upper	Inlet	0.566 m ³ s ⁻¹ (1200 CFM)	<7.0 °C (44.6 °F)
1b	Lower	Inlet		
1c	Upper	Outlet		
1d	Lower	Outlet		
2a	Upper	Inlet	0.425 m ³ s ⁻¹ (900 CFM)	<7.0 °C (44.6 °F)
2b	Lower	Inlet		
3a	Upper	Inlet	0.566 m ³ s ⁻¹ (1200 CFM)	15.9 °C (60.7 °F)
3b	Lower	Inlet		
4a	Upper	Inlet	0.425 m ³ s ⁻¹ (900 CFM)	15.9 °C (60.7 °F)
4b	Lower	Inlet		

3. AIR FLOW DISTRIBUTIONS

3.1 Air Flow Measurements for 0.566 m³s⁻¹ (1200 CFM) Dry Coil Test Case (Test 1)

The Test 1 set of conditions (Table 1) served as the baseline test case. The test apparatus was operated at the manufacturer's rated air flow rate. The water flowing inside the heat exchanger was delivered to the test section at (7.0 ± 0.1) °C ((44.7 ± 0.2) °F) at a rate of (285 ± 0.3) g s⁻¹ to the upper slab and (285 ± 6) g s⁻¹ to the lower slab. The inlet air dew-point was below the inlet water temperature to prevent water vapor condensation on the heat exchanger surface. The heat exchange with each slab was calculated from the water flow rate and the temperature difference between the water entering and exiting each slab of the heat exchanger. During these experiments, the top slab absorbed 5.44 kW of heat from the air, and the bottom slab absorbed 4.47 kW, a difference of 22 %. These basic measurements indicated that there is a significant difference in the amount of air flowing through the two identical slabs of the heat exchanger.

Figure 3 shows the PIV measurements for the approach air flowing to the upper and lower slab; the measurement uncertainty for this and all other data presented in this paper can be found in Yashar and Domanski (2009). The full circles and hollow diamonds represent the data for the air flow to the upper and lower slab, respectively. The horizontal axis in the figure shows the position along the coil, with zero being the base of the coil and the apex at 508 mm; the data plotted is the magnitude of the velocity component perpendicular to the coil. The air flow rate through each coil was calculated by numerically integrating the normal component of velocity from the PIV data, which showed that the top slab received 17.9 % more air than the bottom slab. This is in line with the difference in capacities calculated from the water side measurements. The PIV data for both slabs show the air flow distribution has a generally similar pattern. First, the bottom most 50 mm to 60 mm of the heat exchanger receives no air flow because the mounting bracket blocks off this portion of the heat exchanger's inlet surface. At a certain point afterwards, there is a spike in the amount of air flow incident to the coil. This region is shown at approximately 65 mm to 100 mm on the figure. It is also of interest to note the rapid drop off of air flow near the apex.

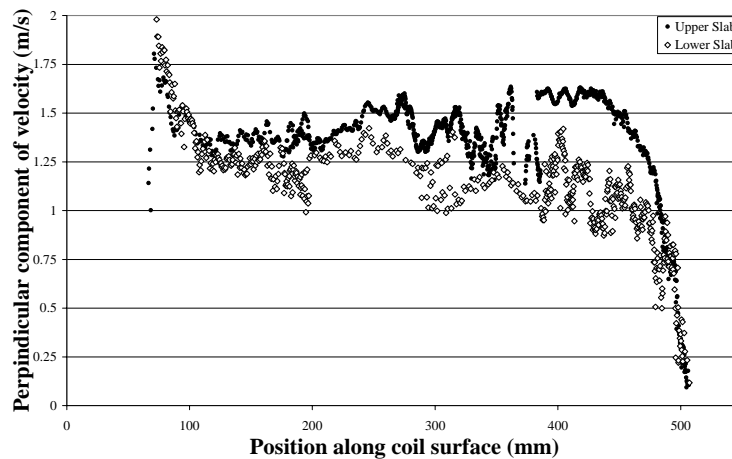


Figure 3 Air Velocity Profiles for Inlet to Dry Coil at 1200 CFM

Tracking the motion of particles entering and leaving the test coil uncovers a lot of detail regarding the local flow patterns. In particular, the velocity profile displays a sinusoidal pattern that corresponds to the presence and absence of a tube in the first depth row. As the air gets closer and closer to the coil, the streamlines will converge towards locations which are gaps between tubes in the first depth row. This causes the approach velocity profile to form a periodic set of velocity peaks and valleys. The magnitude of this sinusoidal component is relatively small at some distance from the inlet side of the heat exchanger, but it is noticeably large on the PIV measurements taken very close to the coil. On the exit side of the coil, air leaves the heat exchanger entirely through the gaps between successive tubes in the last depth row; the sinusoidal component on this side is much larger. In order to determine the general air flow pattern exiting the slab, one must separate out the sinusoidal component; in this manner it appears that the air velocity increases over the first 150 mm, then becomes much more uniform (although slightly increasing still with position along the surface) until the region nearest the apex.

It is interesting to note that the inlet and exit side air velocity patterns are different, which indicates that the air does not pass through the heat exchanger in a perfectly perpendicular direction as previously described in Chwaloski et al. (1989). A plausible explanation for the distinct patterns seen in the different portions of the coil is that they are induced by the geometry of the coil and the features attached to it. In general, the fins impose a lot of flow resistance to the air relative to the other features in the duct. Therefore, in the absence of other features, the air's path of least resistance would be along a streamline that passes perpendicularly through the coil. Since the flow has to turn into the coil at the inlet and into the duct at the coil exit, the path would not be perfectly straight through the entire coil. Most of the middle region of each slab displays a somewhat constant velocity because the air flow resistance along these streamlines is not greatly affected by any of the neighboring regions.

In the region near the mounting brackets of the coil, the air flow must go around the bracket and enter the coil downstream of that point. The portion of the coil inlet just beyond the mounting bracket must therefore be the entrance point for all of the air flowing along the path perpendicular through the coil as well as the entire region of the coil sealed off by the mounting bracket. This is the reason for the velocity spike just beyond the bracket at the coil inlet and the very low velocity near the base of the coil at the coil exit.

The drop off near the apex can be explained by the fact that there is a solid boundary present at the apex of the coil; therefore the air in this region cannot follow the typical flow path either because it cannot begin its turn into the duct before it exits the coil. For this reason, it must turn harder at the exit, which results in greater flow resistance, and therefore the flow velocity is reduced in this region.

3.2 Air Flow Simulations for $0.566 \text{ m}^3\text{s}^{-1}$ (1200 CFM) Dry Coil Test Case (Test 1)

We performed a set of momentum resistance based CFD analyses to simulate the air flow through the test coil under the baseline test case. This method is based on the concept of modeling the heat exchanger as an entity within the flow domain that offers resistance to the flow. We constructed a 2-dimensional model of the test section, which includes both slabs of the heat exchanger, the mounting brackets, and the condensation collection hardware. We assigned momentum resistance coefficients, which were based on pressure drop data acquired during the laboratory experiments, to the nodes residing within the heat exchanger representation. A detailed description of the model and enabling assumptions can be found in Yashar and Domanski (2009).

The simulation results for this test case are qualitatively illustrated in Figure 4, which shows the streamlines through the computational domain; the outlines of the upper and lower slabs of the heat exchanger are highlighted as is the condensation collection hardware. The observed phenomena from the PIV measurements are well represented by these results. The first item to note is the entrance to the heat exchanger, where the area near the base of each slab are somewhat starved for air flow because of the mounting brackets. Also, note that the flow leaving the lower slab must rapidly turn upwards because of the condensation tray, which causes the path through the lower slab to be much more resistive than the path through the upper slab; therefore more streamlines pass through the upper slab.

The PIV data were compared to results of the CFD simulations at 10 mm upstream of the inlet to each slab, the approximate location of the laboratory measurements. The simulations showed very good agreement, matching the velocity data for the upper slab within 15 % over 93 % of the coil surface and the lower slab within 20 % over 82 % of the coil surface. It was a little more difficult to compare the air flow data exiting the heat exchanger because of the large sinusoidal component in the PIV data. Visual examination of the PIV data overlaid with the CFD data, Figure 5, shows that the CFD predicted velocity distribution lines up well with the midpoint of the oscillations suggesting a good fit at the inlet and outlet.

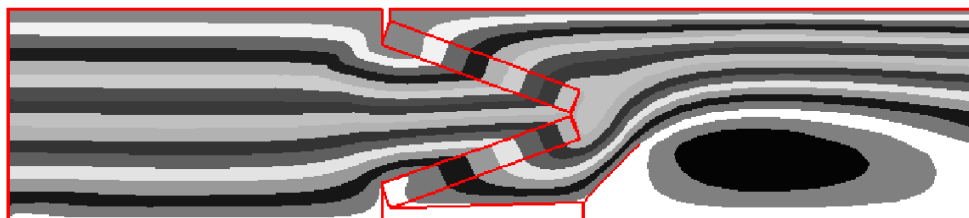


Figure 4 Streamlines for Flow through Dry Coil at 1200 CFM

Since the simulation results of the inlet and outlet of both heat exchanger slabs agreed well with the measured data, we can assume that the CFD solution of the air flow inside the coil is reasonably accurate. Figure 6 shows a map of the velocity magnitude (combined parallel and perpendicular components) overlaid with an array of circles representing the locations of tubes in the heat exchanger. This figure shows that there are a number of tube sites that are exposed to very low air velocities, and these tubes will significantly underperform from a heat transfer point of view.

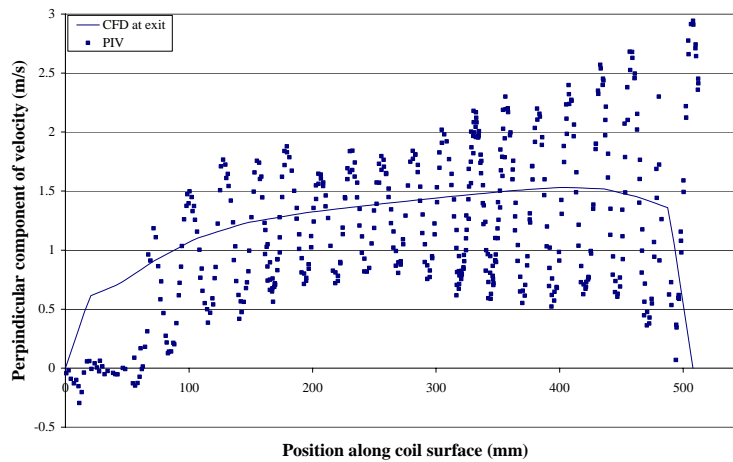


Figure 5 Measured and Predicted Air Velocity Profile for Exit from Top Slab of Dry Coil at 1200 CFM

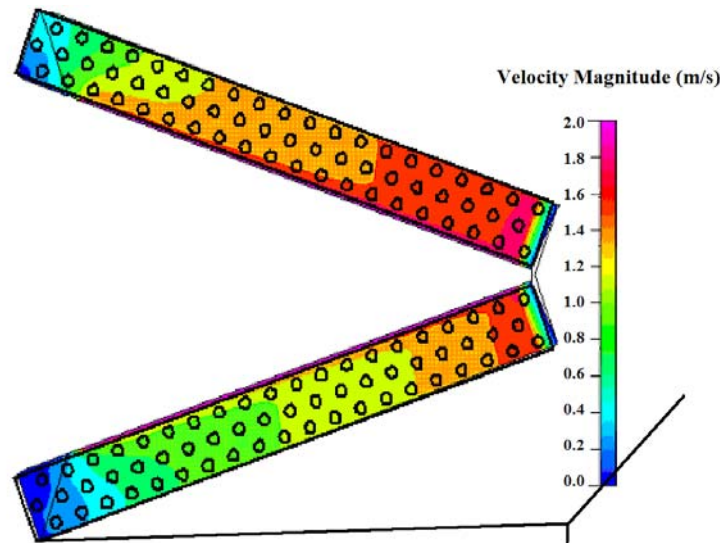


Figure 6 Map of Velocity Magnitude for 1200 CFM Dry Coil

3.3 Air Flow Distribution for $0.425 \text{ m}^3\text{s}^{-1}$ (900 CFM) Dry Coil Test Case (Test 2)

We performed PIV measurements on the inlet and a similar set of CFD experiments for the test coil operating under dry coil conditions with a reduced air flow rate. In this case, the air flow rate was 900 CFM or 75 % of the manufacturer's rated air flow rate. Water was delivered to the test section at $(7.1 \pm 0.1) \text{ }^\circ\text{C}$ ($(44.7 \pm 0.2) \text{ }^\circ\text{F}$) at a rate of $(284 \pm 0.3) \text{ g s}^{-1}$ to the upper slab and $(284 \pm 6) \text{ g s}^{-1}$ to the lower slab. Under these test conditions, the top slab absorbed 4.44 kW of heat from the air and the bottom slab absorbed 3.63 kW, again a difference of 22 %. The PIV data showed a very similar distribution pattern to the full flow dry coil test case, with the only noticeable difference being the magnitude of the air velocity. Numerical integration of the PIV data showed that 18.1 % more air passed through the upper slab than the lower slab, again in line with the previous experiment.

We also performed a CFD simulation using the same methodology as the full air flow test case and found comparable agreement between the simulation and laboratory measurements. In this test case, the CFD data matched the PIV data for the upper slab within 15 % over 78 % of the coil surface and the lower slab within 20 % over 86 % of the coil surface.

3.4 Air Flow Distribution for $0.566 \text{ m}^3\text{s}^{-1}$ (1200 CFM) Wet Coil Test Case (Test 3)

During the next set of experiments, we operated the test coil at the manufacturer's recommended air flow rate, with the air maintained at $(26.7 \pm 0.1) \text{ }^\circ\text{C}$ ($(80.0 \pm 0.2) \text{ }^\circ\text{F}$) and a dew point of $(15.9 \pm 0.6) \text{ }^\circ\text{C}$ ($(60.6 \pm 1.1) \text{ }^\circ\text{F}$). The water circulated through the coil was delivered at an inlet temperature of $(7.4 \pm 0.1) \text{ }^\circ\text{C}$ ($(45.3 \pm 0.2) \text{ }^\circ\text{F}$) at a rate of $(286 \pm 0.3) \text{ g s}^{-1}$ to the upper slab and $(286 \pm 6) \text{ g s}^{-1}$ to the lower slab. The total heat transfer at this flow rate was calculated to be 13.27 kW, of which 7.04 kW was transferred through the top slab and 6.23 kW was transferred through the bottom slab. Again, these measurements show that more heat is transferred through the top slab than the bottom; however, the difference in performance between these two slabs is not as great as with the dry coil tests. This set of data showed that the difference was approximately 13 %.

The air flow distribution measured at the inlet side of the coil bore two major differences to the dry coil test cases. First, the velocity profile measured at each slab tended to be much flatter than that seen on the baseline test case. This is because the flow resistance is much greater in the wet coil since the water held up in the coil restricts the air's path through the coil; a more resistive slab will tend to keep the air flow more uniformly distributed. The other difference is that the lower slab did not display the very large spike in the entrance velocity near the base, as was seen in the other test cases. This is because of the path followed by the water running off the coil. It was observed that the droplets tended to run down the slanted face of the heat exchanger, and more importantly water droplets that formed on the top slab ran towards the apex and then down along the lower slab. Therefore, at any given time, there was more water held in the lower slab since the flow path of the condensation runoff passes through it. Furthermore, the bottom of the lower slab realized the highest concentration of water and therefore offered the highest degree of resistance to air flow. This very large flow resistance prevented the formation of the velocity spike.

Numerical integration of the PIV data showed that 33.1 % more air passed through the upper slab than the lower slab. It is interesting that the slab-to-slab air flow difference is larger for this wet coil condition than the dry coil test while the heat transfer difference between the two slabs is substantially smaller than the other cases. This is because the water running off the coil had a lot more contact with the lower slab and much of the heat transfer realized by the lower slab was used to subcool the water runoff, rather than cooling or dehumidifying the air.

3.5 Air Flow Distribution for $0.425 \text{ m}^3\text{s}^{-1}$ (900 CFM) Wet Coil Test Case (Test 4)

In the final set of experiments, we operated the test coil under low air flow conditions and high humidity. The air was maintained at a flow rate of 900 CFM and a dry bulb temperature of $(26.7 \pm 0.1) \text{ }^\circ\text{C}$ ($(80.1 \pm 0.2) \text{ }^\circ\text{F}$) and a dew point of $(15.7 \pm 0.6) \text{ }^\circ\text{C}$ ($(60.2 \pm 1.1) \text{ }^\circ\text{F}$). The water circulated through the coil was delivered at an inlet temperature of $(7.4 \pm 0.1) \text{ }^\circ\text{C}$ ($(45.2 \pm 0.2) \text{ }^\circ\text{F}$) at a rate of $(285 \pm 0.3) \text{ g s}^{-1}$ to the upper slab and $(285 \pm 6) \text{ g s}^{-1}$ to the lower slab. The total heat transfer under these conditions was calculated to be 11.58 kW, of which 6.12 kW was transferred through the top slab and 5.46 kW was transferred through the bottom slab; a difference of approximately 12 %.

The data from these measurements again showed that the condensation tends to drive the velocity profile towards a more uniform distribution. The data also showed the presence of the velocity spike near the entrance of the lower slab, in contrast to the 1200 CFM wet coil test case. This can be explained, based on visual observation during the laboratory experiments, by a much smaller moisture removal rate for Test 4 than was realized under Test 3. Apparently, this lower rate of condensation runoff did not result in enough water held up in the lower portion of the lower slab to block the region where the velocity spike formed.

Numerical integration of this set of PIV data showed that 15.2 % more air passed through the upper slab than the lower slab, which is interesting because this value lies between the dry coil tests cases and the full flow wet coil test case; this seems logical given the location of the water held up in the coil. When comparing this test case to the dry coil tests, the flow resistance is greater in the wet coil because of the reduced flow area caused by the droplets trapped between the fins. Since the flow through the coil has a higher resistance, the impact of the obstructive features attached to the coil (mounting brackets and condensation collection hardware) is lessened; therefore the air flow is more uniformly split between the two slabs. When comparing this test case to the wet coil full air flow test, the difference in flow resistance is a result of different amounts of water held up in the coils. The condensation rate is much higher for the full flow case and consequently there is a lot more water trapped in the coil under the high flow condition, with a particularly high concentration in the lower region.

4. SUMMARY AND CONCLUSIONS

We measured the velocity distribution of air flowing towards and away from a residential A-shaped finned-tube heat exchanger using Particle Image Velocimetry. We varied the volumetric flow rate and moisture content to examine their effects on the air velocity distribution. We then constructed a CFD model of the test coil, compared our CFD results with the laboratory measurements, and demonstrated that this simple approach can be used to obtain accurate representations of air flow velocity fields.

Our measurement results showed that the presence of the condensation pan caused a significant difference between the amounts of air passing through each slab. In all of the tests, the upper slab received anywhere from 15 % to 33 % more air flow than the lower slab. The upper slab of the heat exchanger also transferred a proportionally larger amount of heat.

The data obtained in this study suggests that a number of options can be taken to improve the performance of A-shaped coil assemblies. We observed flow patterns that indicate substantial low air flow regions exist within the coil due to the geometrical features in the vicinity of the heat exchanger. Specifically, the mounting brackets that hold the coil's position were obstructive to the air flow and resulted in sections encompassing several tubes in the coil to receive little or no air flow. A different design for these brackets could result in better air flow distribution through the coil. As an alternative, eliminating tubes in the no/low air flow regions would result in a smaller heat exchanger, which would reduce material cost to manufacturers, lower the refrigerant side pressure drop, and reduce the refrigerant charge without a performance penalty.

Another option for improving the heat exchanger performance is to redesign the refrigerant circuitry to accommodate the non-uniform in-situ air velocity profile. The knowledge that certain tubes receive more or less air flow should be considered when designing the refrigerant flow path through the slabs. Also, measures should be taken to route more refrigerant to the upper slab than to the lower slab to mitigate the effects of the uneven air split between the two slabs.

REFERENCES

- ASHRAE 1998, *ANSI/ASHRAE Standard 37. Methods of Testing for Rating Unitary Air Conditioning and Heat Pump Equipment*, American Society of Heating, Refrigerating, and Air-Conditioning Engineers, Atlanta, GA.
- Chwalowski, M., Didion, D.A., and Domanski, P.A., 1989, *Verification of Evaporator Computer Models and Analysis of Performance of an Evaporator Coil*, ASHRAE Transactions, 95(1): 1229-1236.
- Payne, W.V. and Domanski, P.A., 2003, *Potential Benefits of Smart Refrigerant Distributors*, (ARTI-21CR/605-200-50-01; 196 p.)
- Domanski, P.A., Yashar, D.A., Kaufman, K.A. and Michalski, R.K., 2004, *An Optimized Design of Finned Tube Evaporators Using the learnable Evolution Model*, HVA&R Research, 10(2): 201-211.
- Domanski, P.A. and Yashar, D.A., 2007, *Optimization of Finned-Tube Condensers Using an Intelligent System*, Int. J. of Refrigeration, 30(3): 482-488.
- Yashar, D.A. and Cho, H.H., 2007, *Air Side Velocity Distributions in Finned Tube Heat Exchangers*, NISTIR 7274, Nat. Inst. of Standards and Technology, Gaithersburg, MD.
- Yashar, D.A., Domanski, P.A., and Cho, H.H., 2008, *Measurement of Air-Velocity Profiles for Finned Tube Heat Exchangers Using Particle Image Velocimetry*, *Int. Refrigeration and Air-Conditioning Conference at Purdue*.
- Yashar, D.A. and Domanski, P.A., 2009, *Particle Image Velocimetry Measurements and CFD-Based Predictions of Air Distribution at Evaporator Inlet and Outlet*, (ARTI Report NO. 07010-01; 67 p.)

ACKNOWLEDGEMENT

This work was sponsored in part by the Air-Conditioning and Refrigeration Technology Institute (ARTI) under contract number ARTI-07010.